

Robot-Assisted Surveillance in Large Environments

Francesco Capezio, Fulvio Mastrogiovanni, Antonio Sgorbissa
and Renato Zaccaria

DIST, Department of Communication Computer and System Sciences, University of Genova, Italy

This paper introduces ANSER, a mobile robot designed to perform surveillance in wide indoor and outdoor areas, such as civilian airports, warehouses or other facilities. The paper describes in details the robot subsystems, focusing on their capabilities in autonomous surveillance, localization and navigation.

Keywords: surveillance, autonomy, localization, navigation

1. Introduction

This paper describes the robot ANSER, which is part of a surveillance system based on both a network of heterogeneous devices and one or more mobile robots. ANSER is meant to be deployed in wide indoor and outdoor areas, such as airports, warehouses and storage facilities.

These sites pose interesting problems for traditional surveillance systems. A *trade-off* must be set between system *specifications* and system *autonomy*. Often, completely autonomous surveillance systems are not what is needed: replacing only selected human operations is usually preferable. This choice is motivated by several reasons: among them, the difficulty of encoding surveillance rules and policies (e.g., how to deal with the situation at hand? which kind of safety protocols should the system use?), the lack of guarantees related to system behavior (e.g., is this the correct behavior to hold? is the robot aware of the consequences of the planned actions?), and the need for humans to be at the core of the decision process (e.g., who is responsible for robot actions?). The design of a real surveillance system starts from system specifications and surveillance objectives. Common

specifications include *area coverage*, *reliability*, *decision making*, *autonomy* and *deployability*.

Area coverage: *Critical areas must be covered by the surveillance system.* In wide environments it is not possible to cover all the *critical* areas in their entirety using fixed devices. Cameras lack in resolution when pointing towards distant areas. Other sensors, like Passive Infra Red (PIR in short) can help if carefully placed, but they cannot be positioned in *traversable* areas such as landing sites.

Reliability: *Patrols must be performed according to predefined policies.* Patrolling operations require active intervention by human personnel during a mission. Human laziness is one of the major causes for lack of security in these cases: very often human patrols are neither completely carried out nor the sequence of visited places varies from patrol to patrol, therefore invalidating surveillance policies.

Decision making: *Anomalies must be carefully investigated.* When an anomaly is detected, a course of action is decided according to both law policies and other considerations related to human safety, security and moral judgement. A completely autonomous system would be *out of control* in such cases, thus not meeting these requirements.

Autonomy and deployability: *The behavior of the surveillance system must be independent from the environment.* This must be guaranteed in all cases. For example, video-based algorithms do not work properly in changing lighting conditions: alternative solutions must

be put into practice to overcome these limitations. On the other hand, localization systems for mobile robots should not rely on *external devices*, such as differential GPS stations, which can not be assumed to be present everywhere: their absence could invalidate the overall system behavior.

These requirements lead to design choices which stress the focus on *interoperability* rather than *complete autonomy*. The name ANSER arises from this approach: ANSER is an acronym for Airport Non-Stop Surveillance Expert Robot, and it is the Latin name for “goose”. Capitoline geese, according to tradition, neutralized a sneak attack by the Gauls during the siege of Rome by simply *rising an alarm*. The ANSER approach is to detect anomalies, to address basic decisions, and then to rise alarms in case that dangerous situations are detected: human personnel can then inspect the critical scenario and decide the most suitable course of action.

In this paper we focus on the mobile robot subsystems, describing in detail how *surveillance*, *localization* and *navigation* are designed to adhere to the proposed philosophy. Section 2 discusses relevant literature. Section 3 introduces the overall surveillance system, focusing on the mobile robot part. Section 4 describes the adopted localization technique, investigating the properties of the augmented state vector approach. Section 5 discusses how robot navigation is affected by the overall design philosophy. Finally, experimental results – obtained in a field set-up at the Albenga Airport (Italy) – are discussed.

2. Related Work

In the following paragraphs, we first discuss mobile robots used for surveillance purposes, and then about algorithms for object detection, localization and navigation in these scenarios.

Mobile Robots for Surveillance. Recently, several autonomous surveillance systems based on mobile platforms have been presented. The goal of MDARS, a joint USA Army-Navy project [1], is to provide multiple mobile platforms performing random patrols in warehouses and storage sites, both indoor and in semi-structured outdoor environments. However, it is immediate to notice that high performances are obtained by over equipping the system with a huge set of

different sensorial devices and by providing adequate on-board computing power to process the huge amount of available data: the localization and navigation subsystems require the joint use of a differential GPS (thus being in contrast with the *autonomy* requirement of surveillance systems), a fiber-optic gyro and the recognition of retroreflective landmarks via a laser-based proximity sensor.

In [2] a network of mobile all-terrain vehicles and stationary sentries are exploited in an autonomous surveillance and reconnaissance system. The vehicles are able to detect and track moving objects, which are classified using learning algorithms, through cameras. Each robot relies for localization on both a differential GPS and an Inertial Measurement Unit (IMU); four networked PCs for navigation, planning, perception and communication are required. In [3] a team of UAVs (i.e., Unmanned Aerial Vehicles) and UGVs pursue a second team of evaders adopting a probabilistic game theoretic approach (see also [4]). Again, the robots need enough computational power to manage a differential GPS receiver, an IMU, video cameras and a color-tracking vision system. In [5] a multirobot surveillance system is presented, describing how a group of miniature robots (called Scouts) accomplishes simple surveillance tasks using an on-board video camera. Because of limitations on the space and power supply available on-board, Scouts rely on remote computers to manage all the resources, to compute decision processes, and finally to provide them with control commands.

Laser-based Object Detection. Algorithms for laser-based people and object tracking range from simple cluster detections to more recent techniques able to classify generic shapes made up of range data. The framework proposed in [13] uses different laser rangefinders, positioned in known locations, to cover a given area: raw scan points associated with moving objects are clustered, and then assigned with a linear movement model. For object tracking, a Kalman filter is used to locate each target. The tracker is able to generate smooth paths even in presence of occluding objects. In [14] laser rangefinders are placed on mobile robots for people tracking. In order to overcome limitations related to the use of Kalman filters (e.g., assumptions related to linearity and unimodal probability distributions), a Bayesian framework is adopted, using a sample-based joint

probabilistic data association filter to track multiple objects at the same time. Finally, more complex features are extracted from range data in [15]: the authors are able to recognize generic features (e.g., legs) given a feature model and training a Bayesian classifier with good results.

Localization and Navigation in Surveillance Robots. With the sole exception of [5], autonomous self-localization and navigation capabilities are fundamental prerequisites in all the robot-based surveillance systems. Starting from a minimal configuration including an IMU and a carrier phase differential GPS receiver [6–9], a common approach to self-localization is to equip the mobile platform with redundant sensory, thus requiring high computational power and complex data filtering. However, system *reliability* and *decision making* are seldom considered. With respect to navigation approaches, issues related to *autonomy* and *reliability* are not usually taken into account. Patrols and laser-based object detection require the system to be robust with respect to localization pitfalls and to be reliable even with minimal sensing requirements. Common approaches in literature [16, 17] require the knowledge of both the distance from the trajectory and the difference between the desired and the current orientation. Furthermore, since they model trajectories using parametric equations, the resulting computational load to model the motion law of the parameters is not negligible.

3. Surveillance

The philosophy of the ANSER project is to integrate heterogeneous sources of information, using different subsystems where the areas to be monitored *allow* for their use. Therefore, near walls and in cluttered areas, a network of fixed sensors can be preferable to mobile robot patrols. However, two issues must be dealt with: (i) the sensor network topology cannot be easily modified according to specific needs, and (ii) in some areas sensors must be easily removable when other activities take place (e.g., cameras cannot be placed in the middle of a runway where planes take-off!). Although mobile robots are more expensive, they require more complex algorithms for data processing, and have well-known problems related to power supply, nonetheless they can move where needed, thus increasing *deployability* and

adaptability. In particular, in open spaces, the superior mobility, the sensing range and precision of a mobile robot equipped with a laser rangefinder are expected to produce more accurate results. With respect to these considerations, a system can be envisaged taking *complementary subsystems* and a *two-layer decision making* framework into account.

Complementary subsystems. The overall surveillance system is made up of two components: the former is a standard network of heterogeneous devices, exploiting video cameras, microphones or PIR sensors, thus being able to detect anomalies according to sensors' range, whereas the latter is a collection of mobile robots, whose aim is to address system adaptability and to increase *area coverage*. In a sense, the traditional surveillance paradigm is extended by adding mobile platforms able to *transport sensors where needed*. This approach increases the autonomy and the range of action of the overall system thereby reducing the need for human intervention in many situations.

Two-layer decision making. When performing patrolling operations the system does not autonomously take any course of action for anomalies. However, basic tasks (e.g., checking if doors are correctly closed or if humans can identify themselves through RFID badges) can be carried out as long as things go smooth. Otherwise, the mobile robot will simply *detect* anomalies (e.g., presence of objects in *critical* areas, misplaced objects and furniture, or personnel without required permissions, etc.), and it will be teleoperated in order to further investigate the situation using human cognitive capabilities.

In particular, an intelligent (possibly *semi-autonomous*) supervisor maintains a coherent world model by dividing the whole workspace into different areas: a number of areas are assigned to fixed distributed devices, whereas others are monitored by mobile robots. Whenever needed, the system is able to *orchestrate* the coordinated behavior of both devices and robots. For example, it could plan a course of action for a robot in order to investigate the situation: the robot could be asked to reach the area where the anomaly has been detected in order to provide a remote operator with camera images, or to use the laser rangefinder to gain a fine grained resolution image of a particular object. In the following paragraphs, we specifically focus on the capabilities of a single mobile robot.

3.1. Laser-based Surveillance

Laser rangefinders were initially designed for improving safety and security in factories: the idea is to monitor an area of interest (e.g., in the proximity of a machine tool) where the presence of people or objects should cause an immediate arrest. In a similar spirit, a very conservative laser-based surveillance algorithm is used in ANSER to identify anomalies.

First, during the design phase, the whole region to be monitored by the mobile robot (e.g., in Figure 1, an airport terminal and runways) is split into n convex polygonal areas $\{A_i\}$. Each polygon defines a *critical area*. Next, when performing patrolling operations according to surveillance policies, clusters $\{C_j\}$ are periodically extracted from raw laser measurements, which can be as simple as point features or line features, or complex as legs or body shaped objects. Specifically, clusters of points are represented by a *center of mass* $\mathbf{c}_j \in \mathbf{R}^2$ and a *covariance matrix* $m_j \in \mathbf{R}^{2 \times 2}$.

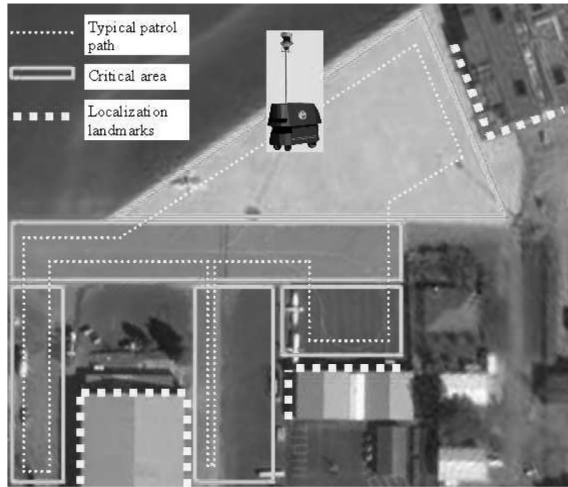


Figure 1. Patrol rounds in an airport scenario.

In our scenario, the system assumes that the monitored area must be empty and every cluster that is detected inside it must be considered a potential threat. The overall surveillance activities performed by the ANSER mobile robot are carried out by concurrent agents which are charged of performing different tasks: laser data acquisition and filtering, objects detection, etc. However, for the sake of explanation, it is possible to describe the robot behavior through Algorithm 1. It is worth noticing that this structured

behavior *emerges* from the interaction of the different involved agents, and there is by no means any centralized supervision.

Algorithm 1 laser_based_surveillance()

```

Require: true  $\leftarrow$  patrolling_started()
Ensure: {true,false}  $\leftarrow$  object_detection()
1: while false  $\leftarrow$  patrolling_completed() do
2:   navigate_to_next( $A_i$ )
3:    $\{C_j\} \leftarrow$  sense_and_associate()
4:   if  $C_j \in \{A_i\}$  then
5:     patrolling_suspended()
6:     badge_id  $\leftarrow$  scan_rfid()
7:     if authorized_rfid(badge_id) then
8:       patrolling_resumed()
9:     else
10:      alert_supervisor()
11:      enter_teleoperated_mode()
12:      if telep_command  $\leftarrow$  manually_operate then
13:        manually_operated()
14:      end if
15:      if telep_command  $\leftarrow$  map then
16:        map_object( $c_j$ )
17:      end if
18:      if telep_command  $\leftarrow$  resume then
19:        patrolling_resumed()
20:      end if
21:    end if
22:  end if
23: end while

```

The robot surveillance task consists of carrying around the laser rangefinder, thus visiting all the critical areas in sequence (line 2, see also Section 5). The robot is provided with a map of the patrolling area: therefore, it has knowledge of known or previously mapped object locations and object-free areas. While navigating, if an anomaly C_j is detected, a tentative association to previously mapped objects $\{O_i\}$ is carried out through the minimization of the Mahalanobis distance $M(C_j, O_i)$ between the actual cluster and all the previously mapped objects, i.e.,

$$M(C_j, O_i) = \sqrt{(\mathbf{c}_j - \mathbf{o}_i)^T m_j^{-1} (\mathbf{c}_j - \mathbf{o}_i)} \quad (1)$$

where \mathbf{o}_i is the baricentre of one mapped object. If a suitable O_i is found, C_j is recognized as a previously detected object. Otherwise, the robot stops (line 5). It is worth noting that centers of mass are compared with respect to a global reference frame, thus ultimately relying on self-localization (see Section 4). As a consequence, it is fundamental to maintain errors in self-localization under certain bounds.

Anomalies depend on the particular area: as previously discussed, potential anomalies encompass misdisplaced objects (e.g., opened doors which should be closed), unforeseen obstacles in areas which are assumed to be free, and moving objects. With respect to misdisplaced objects, their status can be easily recognized using scan-matching techniques. However, a more interesting case is posed by unknown objects. Within monitored environments, it is usually common to assume the availability of RFID enabled badges and tags. Humans and objects can be given RFID identification capabilities, in order to be easily recognized by the system. Therefore, the robot silently scans for RFID readings: if the detected object can provide a RFID identification tag which classifies it as *authorized*, the mobile robot simply resumes its patrol (lines 6 to 8); otherwise, it warns the intelligent supervisor that an unexpected object has been detected (line 10). At this point, a human supervisor can manually teleoperate the robot (line 13), using video feedback provided by an onboard pan/tilt/zoom video camera to further investigate the situation. During this operation, data can be collected from the scene: estimated object position, shape, dimension, etc. Finally, if the situation is classified by the supervisor as *normal* (e.g., an object left unattended, a vehicle parked in an unusual place) the object is mapped (line 16), and the robot resumes its patrol (line 19), ignoring the same object in the future if the position, shape and dimensions match.

4. Localization

In surveillance scenarios, mobile robots are required to patrol wide regions and to devote special care to *critical* areas, according to given policies. In order to meet *autonomy* requirements, the ANSER localization subsystem relies only on a single non-differential GPS receiver and a laser rangefinder.

Unfortunately, GPS measurements are corrupted by error sources introducing highly *colored* noise with significant low-frequency components, which can be modeled as a non-zero mean value (i.e., a *bias*) in GPS errors slowly varying in time [9]. The analysis of both longitude and latitude data collected for 24 hours at a fixed location clearly shows this effect: considering the Fast Fourier Transform (FFT in short) of

GPS longitude and latitude data, low-frequency components can be noticed, corresponding to a slow variation of the signal over time. By estimating this bias in GPS measurements, one can expect to improve GPS data precision, therefore making robot localization more accurate.

To this purpose, an augmented state vector \mathbf{x} is defined, comprising the x , y , and θ components of the robot pose, as well as the x_{gps} and y_{gps} components of the low-frequency bias. Since the colored components are then separated from additive white gaussian components of GPS noise (i.e., they are comprised in the state vector), an Extended Kalman Filter (EKF in short) can be applied [10].

With respect to laser-based localization, the *a priori* map of the environment includes, in addition to objects $\{O_i\}$ which have been detected by the surveillance system during previous patrols, a collection of *oriented* line segments $\{m_i\}$. Notice that line segments are represented through their implicit equation in the form $m_i(a, b, c) = 0$, and are fed to a self-localization process which runs concurrently with laser-based surveillance, but requires features to be stable across different runs. In this sense, the map has multiple layers, each layer having different characteristics and a different purpose.

When navigating indoor, the laser-based localization subsystem simply updates the robot pose by comparing the given map with features detected by the laser rangefinder. The mobile robot is equipped with two laser rangefinders (see Figure 5 at the top left): the former – used for surveillance – is hidden within the chassis and it is located about 50 cm above the ground, whereas the latter – used for self-localization – is located on top of a pole about 2 m high. As soon as new laser measurements are available, (i) *line extraction* produces a number of lines $\{l_j\}$ using a common Split & Merge algorithm; (ii) the Mahalanobis distance associated with each tuple (l_j, m_i) is computed; (iii) for each l_j , the line m_i for which such a distance is minimum is selected and fed to the EKF, which can then update the robot pose using a line measurement model and the actual measure l_j [11].

When moving outdoor, lines within the *a priori* map mostly correspond to external walls of buildings. In this situation, a smaller number of features are available (see Figure 1), since the

robot mostly traverses areas where no lines are detected at all. However – when line features are available – their contribution is sufficient to estimate the full state vector and – under a number of assumptions – the pose estimate is still valid even when the rangefinder does not provide any further information.

4.1. An Augmented State Vector

The approach relies on the idea of including the GPS bias in the state to be estimated. The resulting augmented state vector is shown in Equation 1.

$$\mathbf{x}^T = \begin{bmatrix} x_1 & x_2 & x_3 & x_4 & x_5 \\ x & y & \vartheta & x_{bias} & y_{bias} \end{bmatrix} \quad (2)$$

It includes the robot position and orientation with respect to a fixed frame, and the two components of the GPS bias. The system can be modeled with the following differential equations:

$$\begin{aligned} \dot{x}_1 &= \frac{R}{2} [(u_1 + w_1) + (u_2 + w_2)] \cos x_3 \\ \dot{x}_2 &= \frac{R}{2} [(u_1 + w_1) + (u_2 + w_2)] \sin x_3 \\ \dot{x}_3 &= \frac{R}{D} [(u_1 + w_1) - (u_2 + w_2)] \\ \dot{x}_4 &= u_3 + w_3 \\ \dot{x}_5 &= u_4 + w_4 \end{aligned} \quad (3)$$

with

$$\mathbf{u}^T = [u_1 \ u_2 \ u_3 \ u_4] = [\omega_r \ \omega_l \ 0 \ 0] \quad (4)$$

and

$$\mathbf{w}^T = [w_1 \ w_2 \ w_3 \ w_4] = N(0, Q) \quad (5)$$

The first three rows in Equation 3 describe the vehicle unicycle kinematics: u_1 and u_2 are the rotational speed ω_r and ω_l of the right and left rear wheels; w_1 and w_2 are zero-mean, AWG noise allowing to model non-systematic errors in control and odometric reconstruction. R is the wheels radius, and D is the distance between wheels. The fourth and fifth rows in Equation 3 describe how bias changes in time. However, since this is obviously unknown, the bias is assumed to be constant (i.e., $u_3 = u_4 = 0$), and the variation of x_{bias} and y_{bias} in time is assumed to depend exclusively on the noise w_3 and w_4 .

After integrating the dynamic equations of the system through a standard Euler approximation with an appropriate step size, the system

can be described at instant k through the following finite difference equations in the form $\mathbf{x}_k = f(\mathbf{x}_{k-1}, \mathbf{u}_k, \mathbf{w}_k)$:

$$\begin{aligned} x_{1,k} &= x_{1,k-1} + \frac{R(u_{1,k} + w_{1,k} + u_{2,k} + w_{2,k})\Delta t}{2} \cos x_{3,k-1} \\ x_{2,k} &= x_{2,k-1} + \frac{R(u_{1,k} + w_{1,k} + u_{2,k} + w_{2,k})\Delta t}{2} \sin x_{3,k-1} \\ x_{3,k} &= x_{3,k-1} + \frac{R(u_{1,k} + w_{1,k} - u_{2,k} - w_{2,k})\Delta t}{D} \\ x_{4,k} &= x_{4,k-1} + w_{3,k} \\ x_{5,k} &= x_{5,k-1} + w_{4,k} \end{aligned} \quad (6)$$

Equation 6 can be used to estimate the state and the covariance in the prediction phase of the Extended Kalman Filter at step k as:

$$\begin{aligned} \hat{\mathbf{x}}_k^- &= f(\hat{\mathbf{x}}_{k-1}, \mathbf{u}_k, 0) \\ P_k^- &= A_k P_{k-1} A_k^T + W_k Q_{k-1} W_k^T \end{aligned} \quad (7)$$

Notice that, even if the dynamics of the bias is assumed constant, and hence the corresponding components of $\hat{\mathbf{x}}_k^-$ are left unchanged in the prediction phase, the same is not true for the estimated covariance P_k^- , which is updated in the prediction phase according to the EKF equations and increases at each iteration depending on the noise covariance Q . Since the uncertainty of the estimated bias increases with time, the predicted values $\hat{x}_{k,4}^-$ and $\hat{x}_{k,5}^-$ are very likely to be updated in k if new measurements are available (i.e., in the correction phase of the EKF), thus finally producing an estimate that varies in time as well, and hopefully approximates the actual bias in GPS measurements. Remember that in the measurement update phase, it holds:

$$\begin{aligned} \hat{\mathbf{x}}_k &= \hat{\mathbf{x}}_k^- + K_k(z_k - h(\hat{\mathbf{x}}_k^-, 0)) \\ P_k &= (I - K_k H_k) P_k^- \\ K_k &= P_k^- H_k^T (H_k P_k^- H_k^T + V_k R_k V_k^T)^{-1} \end{aligned} \quad (8)$$

In other words, the corrections performed on each component of the state $\hat{\mathbf{x}}_k$ (first equation) depend on the kalman gain K_k , which (third equation) directly depends on the state covariance P_k^- (and inversely depends on the measurement covariance R_k). Finally, since the state equations are not linear, A_k is computed as the Jacobian matrix of partial derivatives of f with respect to x , and W_k is computed as the Jacobian matrix of partial derivatives of f with respect to w .

Measurements \mathbf{z}_{gps} can be modeled by a non linear function of the state, because the relationship between georeferenced data (i.e., latitude and longitude) and the estimated x - and y -coordinates varies with the latitude itself, as a consequence of the non planarity of the earth surface:

$$\mathbf{z}_{gps}^T = [z_1 \quad z_2] = [\text{long} \quad \text{lat}] \quad (9)$$

which can be expressed as a non-linear function of the state (in discrete form):

$$\begin{aligned} z_{1,k} &= f_{\text{long}}(x_{2,k}) \cdot (x_{1,k} + x_{4,k}) + v_{1,k} \\ z_{2,k} &= f_{\text{lat}}(x_{2,k}) \cdot (x_{2,k} + x_{5,k}) + v_{2,k} \end{aligned} \quad (10)$$

where $v_{1,k}$ and $v_{2,k}$ can now be modeled as zero-mean AWG noise with variance R_1 and R_2 , and the scale factors $f_{\text{long}}(x_{2,k})$ and $f_{\text{lat}}(x_{2,k})$ depend on current latitude.

Conversely, for each line feature l_j originating from laser data, the map line m_i that best matches l_j can be expressed using two parameters representing, respectively, the distance ρ from the robot and the angle α between the line itself and the robot's heading [11]:

$$\mathbf{z}_{laser}^T = [z_3 \quad z_4] = [\rho \quad \alpha] \quad (11)$$

By considering the implicit equation to compute the distance between a line and a point, the measurement model turns out to be linear:

$$\begin{aligned} z_{3,k} &= (a_i x_{1,k} + b_i x_{2,k} + c_i) / \sqrt{a_i^2 + b_i^2} + v_{3,k} \\ z_{4,k} &= \tan^{-1}(-a_i/b_i) - x_{3,k} + v_{4,k} \end{aligned} \quad (12)$$

where a_i , b_i and c_i are the parameters characterizing the implicit equation of m_i , and $v_{3,k}$ and $v_{4,k}$ can be modeled as zero-mean AWG noise with variance R_3 and R_4 .

Whenever new GPS or laser measurements are available, they are fused with the prediction (Equation 7) to produce a new estimate (Equation 8), thus reducing displacement errors which inherently characterize odometry and providing also a new estimate for the GPS bias. Notice that, since GPS data are not a linear function of the state, it is necessary to compute H_k in Equation 8 as the Jacobian matrix of partial derivatives of h with respect to x . On the contrary, the dependence of h from noise is linear both for the GPS and for the laser scanner, hence we set $V_k = I$.

In principle, observations are provided concurrently by both the GPS and the laser rangefinder. This happens when the robot is operating outdoor *and* landmarks for laser-based self-localization, for example buildings, are available in the neighborhoods. However, in open spaces, GPS is usually the only sensor providing information, since building walls could be so distant to be undetectable by laser rangefinders. Therefore, two cases must be dealt with separately, by considering (i) corrections provided by the GPS alone, and (ii) corrections provided concurrently by the GPS and the laser-scanner. A formal observability analysis is outside the scope of this paper. However, by writing the Kalman observability matrix O_k , with $O_k^T = [H_k^T \quad A_k^T H_k^T \quad \dots A_k^{T4} H_k^T]$, it is straightforward to demonstrate that:

- (i) when only GPS data are available, only the subspace defined by $(x_1 + x_4, x_2 + x_5, x_3)$ is fully observable: the estimated robot's position has a permanent error that depends on the current estimate of the GPS bias. The robot's orientation x_3 can be corrected only when the robot is moving.
- (ii) the whole state \mathbf{x} is *fully* observable when at least one GPS measurement *and* two non parallel laser measurements are considered in cascade [12].

The former case is particularly interesting: in this case, innovation due to GPS measurements is distributed by the Kalman gain onto x , y , x_{bias} and y_{bias} according to the current value of the state covariance matrix P in such a way as to maximize likelihood. By focusing, for example, on x and x_{bias} , let's assume that P_k can be written as follows:

$$P_k = \begin{bmatrix} p_{11} & \cdots & p_{14} & \cdots \\ \vdots & \ddots & \vdots & \\ p_{41} & \cdots & p_{44} & \cdots \\ \vdots & & \vdots & \ddots \end{bmatrix} \quad (13)$$

The term $p_{11} = \sigma_{x_1}^2$ is the variance of $x_1 = x$, $p_{44} = \sigma_{x_{bias}}^2$ is the variance of $x_4 = x_{bias}$, and finally $p_{14} = p_{41} = \sigma_{x, x_{bias}}$ is the corresponding covariance. When taken together, they define the covariance matrix $P_{k, [x_1 x_4]}$ of the vector $[x_1 \quad x_4]$ which can be graphically represented as an ellipse, whose axes have the orientation of $P_{k, [x_1 x_4]}$'s eigenvectors and the length of the corresponding eigenvalues.

See, for example, Figure 2 (ellipses correspond to subsequent iterations): starting from an initial situation in which $p_{11} = 1, p_{44} = 1, p_{14} = p_{41} = 0$ (i.e., x_1 and x_4 are not correlated), $P_{k,[x_1,x_4]}$ is updated through the EKF. However, if only GPS measurements are available, the linear composition $x_1 + x_4$ is observable whereas each single component is not. This means that p_{11} and p_{44} initially decrease, but they do not tend to zero (which would happen if each single component would be observable). More important, p_{14} and p_{41} decrease down to a constant value < 0 after each iteration, i.e., x_1 and x_4 tend to be more and more correlated (the minor axis of the corresponding ellipse tends to zero, and ellipse's axes tend not to be aligned with the main axes).

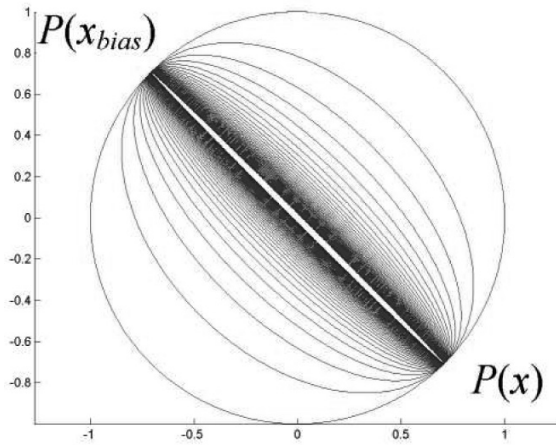


Figure 2. State partially observable.

If, at a given instant, laser measurements are available (see Figure 3), x_1 is immediately corrected, and x_4 is consequently updated as well (i.e., both p_{11} and p_{44} tend to zero, as well as the axes of the corresponding ellipse). Finally, after both p_{11} and p_{44} have been reduced, the latter increases faster than the former in the prediction phase of the EKF (Equation 7), since it is reasonable to assume that the error made in modeling the GPS bias as constant (Equation 3) increases faster than the odometric error. The result is that – after a landmark has been observed – the innovation is mostly projected onto x_{bias} and y_{bias} : when the robot has traveled a long path without observing any landmark, corrections are adequately distributed onto the state components only if the actual GPS bias changes slowly, and given that a new landmark for laser-based re-localization will soon be available.

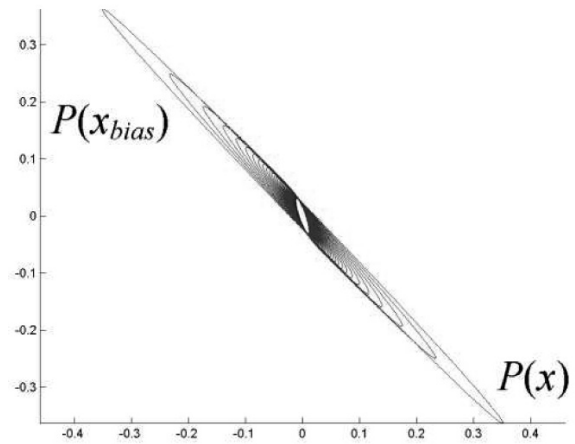


Figure 3. State completely observable.

5. Navigation

The approach adopted for localization allows an accuracy which is sufficient to reliably recognize objects and persons which are not stored in the map through the laser-based surveillance algorithm (this will be shown in the next Section). However, for the purpose of navigation, the resulting positioning accuracy turns out to be inadequate when adopting a standard approach for trajectory tracking. In particular, since most of the time only the GPS is available for positioning, the orientation is properly estimated only when the robot is moving at high speed, thus being unreliable for feedback control. When this happens, an oscillatory behavior around the imposed trajectory can be observed, which must be obviously avoided. To this purpose, we have designed a new control model which allows to regulate to zero *the distance from the trajectory* as well as *the difference between the vehicle's orientation and the tangent to the curve*, and it is proven to be *asymptotically stable*. However, it is different from other models in literature in the following two issues:

- (i) only the distance $D(x, y)$ between the vehicle and the trajectory is measured and fed to the controller, whereas most approaches require to measure both the distance *and* the robot's orientation.
- (ii) the trajectory is expressed through the implicit equation of the curve in the form $t(x, y) = 0$.

For the sake of brevity, we consider here only the case that the curve corresponds to a straight line connecting subsequent via-points, which is a very reasonable approach when traversing outdoor areas. However, the model has been demonstrated to be asymptotically stable for each curve which can be expressed through its implicit equation.

By referring to the continuous-time model of the vehicle kinematics (first three rows in Equation 3), it is now assumed – to simplify the discussion – that control inputs U_1 and U_2 correspond to the robot's linear and rotational velocity, instead of the wheels velocity ω_r and ω_l . That is, by ignoring process noise, we define

$$U_1 = \frac{R}{2} (\omega_l + \omega_r), \quad U_2 = \frac{R}{D} (\omega_l - \omega_r) \quad (14)$$

which yields:

$$\begin{aligned} \dot{x}_1 &= U_1 \cos x_3 \\ \dot{x}_2 &= U_1 \sin x_3 \\ \dot{x}_3 &= U_2 \end{aligned} \quad (15)$$

Without losing generality, we assume that the trajectory to be followed is a straight line which lies onto the x -axis of the reference frame (Figure 4): in this case, $x_2 = y$ obviously corresponds to the distance to the line, and $x_3 = \theta$ is the difference between the orientation of the robot and the orientation of the line (which is zero). $x_1 = x$ increases as the robot moves along the line. It can be demonstrated that, to achieve asymptotic stability, it is sufficient to set control inputs as follows:

$$\begin{aligned} U_1 &= \bar{U}_1 \\ U_2 &= K_p(-x_2 - \dot{x}_2) \end{aligned} \quad (16)$$

The underlying idea is simple. If the robot moves with a linear speed U_1 , the component of

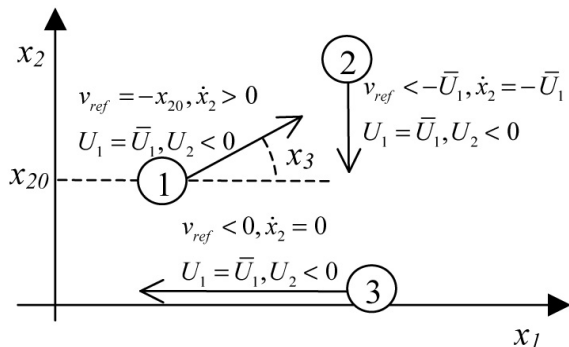


Figure 4. Tracking a straight trajectory.

U_1 along x_2 is $\dot{x}_2 = U_1 \sin x_3$. This is called *approaching velocity*: in situation 1 in Figure 4, \dot{x}_2 is positive since x_3 increases counter-clockwise. Notice that the *approaching velocity* \dot{x}_2 can be increased (up to a maximum value U_1) or decreased (down to a minimum value $-U_1$) by controlling x_3 , which – on its turn – requires to operate on the rotational speed U_2 . In particular, Equation 16 sets the rotational speed U_2 as proportional to the difference between a *reference approaching velocity* $v_{ref} = -x_2$ and the real *approaching velocity* \dot{x}_2 . The *reference approaching velocity* has the following properties:

- (i) when $x_2 = 0$, $v_{ref} = 0$ as well (the robot lies on the trajectory);
- (ii) when $x_2 > 0$, $v_{ref} = -x_2$ is negative (heading downward in Figure 4);
- (iii) when $x_2 < 0$, $v_{ref} = -x_2$ is positive (heading upward in Figure 4).

The linear speed U_1 is a free variable and can have a generic profile $\bar{U}_1(t)$ (given that it satisfies kinematics and dynamics constraints). We assume in the following that $\bar{U}_1(t) = \bar{U}_1$ is constant: since we are dealing with a regular, time invariant system, it is sufficient to demonstrate that the system is stable for every constant input \bar{U}_1 to deduce stability for a generic velocity profile $\bar{U}_1(t)$.

Since x_1 is obviously never in equilibrium (the robot moves along the line), we are interested only in the stability of x_2 and x_3 , which requires to consider a system composed of the second and third rows in Equation 15:

$$\begin{aligned} \dot{x}_2 &= \bar{U}_1 \sin x_3 \\ \dot{x}_3 &= K_p(-x_2 - \bar{U}_1 \sin x_3) \end{aligned} \quad (17)$$

Equilibrium points are given by the solutions of

$$\begin{aligned} 0 &= \bar{U}_1 \sin x_3 \\ 0 &= K_p(-x_2 - \bar{U}_1 \sin x_3) \end{aligned} \quad (18)$$

Equilibrium points correspond to the set $\{(x_2 = 0, x_3 = k\pi) | k \in \mathbf{Z}\}$, i.e., when the distance from the line is null and the robot is oriented along the line. It is necessary to demonstrate that points in the set $\{(x_2 = 0, x_3 = 2k\pi) | k \in \mathbf{Z}\}$ are stable equilibrium points, whereas $\{(x_2 = 0, x_3 = (2k + 1)\pi) | k \in \mathbf{Z}\}$ are not (the robot is moving along the line but in the wrong direction). By considering – for the moment – the only point

$(x_2 = 0, x_3 = 0)$, a C^1 Lyapunov function can be defined, i.e.,

$$V(x_2, x_3) = \frac{K_p x_2^2}{2} + \bar{U}_1(1 - \cos x_3) \quad (19)$$

which is locally positive definite and $V(0, 0) = 0$. Its derivative with respect to time, i.e.,

$$\begin{aligned} \dot{V}(x_2, x_3) &= K_p x_2 \bar{U}_1 \sin x_3 \\ &\quad + \bar{U}_1 \sin x_3 K_p (-x_2 - \bar{U}_1 \sin x_3) \\ &= -K_p \bar{U}_1^2 \sin^2 x_3 \end{aligned} \quad (20)$$

is negative semidefinite, since it does not depend on x_2 and hence $\dot{V}(x_2, x_3) = 0$ for all points in the set $\{(x_2 = \bar{x}_2, x_3 = 0) | \bar{x}_2 \in \mathbb{R}\}$ (corresponding to the x_2 -axis). This is sufficient to state that the equilibrium point $(x_2 = 0, x_3 = 0)$ is locally stable: to prove asymptotic stability, it is possible to apply the LaSalle's invariance principle. This latter part of the demonstration is not shown here for the sake of brevity: however, it is straightforward to notice that the origin is the only possible stable point. In fact, by considering a generic point $(x_2 = \bar{x}_2, x_3 = 0)$ along x_2 -axis, the second row in Equation 17 becomes:

$$\dot{x}_3 = K_p(-\bar{x}_2 - \bar{U}_1 \sin 0) \quad (21)$$

That is, Equation 21 drives the system outside x_2 -axis unless $\bar{x}_2 = 0$, which happens only in the origin. These results can be extended to all equilibrium points in the set $\{(x_2 = 0, x_3 = 2k\pi) | k \in \mathbb{Z}\}$ by considering x_3 's periodicity.

We still need to demonstrate the instability of points in the set $\{(x_2 = 0, x_3 = (2k + 1)\pi) | k \in \mathbb{Z}\}$ (which guarantees that the vehicle cannot head towards the wrong direction). This can be done by introducing an accessory state variable $x_6 = x_3 - \pi$, by writing the corresponding state equations, and by demonstrating that the equilibrium point $(x_2 = 0, x_6 = 0)$ is unstable through the Lyapunov theorem. Once again, the demonstration is not shown here. Consider however situation 3 in Figure 4: it is straightforward to see that, when the vehicle is heading towards the wrong direction and $x_2 \neq 0$, the rotational speed U_2 is sufficient to make the robot diverge from its current trajectory.

Finally, consider situation 2 in Figure 4. The control law in Equation 16 has a problem: when

the distance from the curve (and hence the *reference approaching velocity* v_{ref}) is bigger than the maximum *approaching velocity* \dot{x}_2 (whose absolute value is \bar{U}_1), the *reference approaching velocity* cannot be achieved simply by controlling U_2 . This can cause the vehicle to converge to an equilibrium point $\{(x_2 = 0, x_3 = 2k\pi)\}$, $k \neq 0$ after performing some loops. To avoid this, it is sufficient to saturate v_{ref} to a minimum value $-\bar{U}_1$ when $x_2 > \bar{U}_1$ and to a maximum value \bar{U}_1 when $x_2 < -\bar{U}_1$. By substituting the new value of v_{ref} in Equation 17, asymptotic stability can be easily demonstrated through the Lyapunov's and LaSalle's theorems, as previously.

6. Experimental Results

Figure 5 shows a number of snapshots taken from a video recorded for the first public demonstration of ANSER in October 2006¹. The robot is performing patrol rounds, both outdoor and indoor (see Figure 5, top line). When either the robot or distributed devices (e.g. Passive Infrared Sensors are used in this scenario) detect an unexpected object or a potential intruder, an RFID emission is immediately searched for.



Figure 5. Robot ANSER at the Albenga Airport.

¹ The video is available at www.laboratorium.dist.unige.it.

If it is not found, a *question mark* appears in the human supervisors interface, meaning that *further investigation is required* (see Figure 5 on the bottom left). The human supervisor – possibly operating in a room far away – is alerted (see Figure 5 on the mid left), and can remotely control the robot to better assess the situation. Video feedback is provided through the pan/tilt/zoom camera on-board the robot (see Figure 5 on the mid right). In this case, an abandoned luggage is found, and the supervisor simply updates the question mark in the GUI with a different symbol, meaning *object to be removed* (handling it with care...). The robot can then continue its patrolling operations. In Figure 5 at the bottom, a different situation is shown: the robot has detected a moving person, and *asks* him to exhibit his credentials to check if he is allowed to be in that area. If the person is provided with a RFID badge (which happens to be true in this case), the robot simply resumes its patrol, without alerting the human supervisor.

6.1. Localization

For what concerns the localization subsystem, many experiments in simulation (Figure 6), as well as at the Albenga Airport and in our Campus (Figure 7) have been performed. In simulated tests, landmarks for laser-based localization are available along the path every 50, 100, or 200 m depending on the experiment. Odometry and laser errors are simulated, whereas *real* GPS data belonging to a previously acquired data set are used. During the localization tests at the Albenga Airport, the robot is manually driven at 1.0 m/s along a path that is about 500 meters long. Walls for laser-based localization are *visible* only in a very limited area of the Airport (i.e., buildings walls in Figure 1), which forces the robot to rely exclusively on GPS most of the time. During the tests in

| land. dist. | A-tests | B-tests | C-tests |
|-------------|---------|---------|---------|
| 50m | 1,744 | 0,303 | 1,632 |
| 100m | 1,938 | 0,76 | 1,844 |
| 200m | 2,024 | 1,256 | 1,934 |

Figure 6. Simulated localization tests.

| scenario | A-tests | B-tests | C-tests |
|----------------|---------|---------|---------|
| <i>Campus</i> | 3,02 | 1,84 | 2,96 |
| <i>Airport</i> | 2,3 | 1,83 | 2,22 |

Figure 7. Localization tests.

our Campus, the robot is driven back and forth along a path which is about 100 meters long, and a new landmark for localization is available every 200 meters. Under these conditions, tests have been performed in three modalities: (i) A-tests correspond to localization without including the bias in the state vector, i.e., by modeling the GPS noise as AWGN and by using laser measurements (when available) to correct only the robot’s position; (ii) B-tests are performed by including the GPS bias in the augmented state vector, i.e., by using laser measurements to estimate the bias and letting the EKF update this estimate even when laser measurements are not available (i.e., when the state is not fully observable); (iii) C-tests are performed by estimating the bias *only when* laser measurements are available (i.e., when the state is fully observable), and using this estimate (without updating it) to correct GPS errors when laser measurements are not available. Notice that case (ii) corresponds to the approach described in Section 4, whereas case (iii) describes a control test, i.e., to verify whether updating the bias, even when the state is not fully observable increases localization accuracy.

Different experimental runs have been performed, by recording the robot estimated position in a number of selected locations along the path, and by computing the difference between the actual and the estimated robot’s position. Figures 6 and 7 report the average positioning error $E(\sqrt{(\hat{x} - x)^2 + (\hat{y} - y)^2})$. In all cases, the positioning error in B-tests is lower, whereas C-tests yield approximately the same accuracy as A-tests. However, the increment in performance is not that evident at Albenga Airport. A deeper analysis reveals that – in this latter scenario – GPS errors are lower in the first place, which influences the final positioning error: this is due to the absence of tall buildings, which are known to be one of the major causes of signal occlusions and multi-path effects, which severely affect the GPS accuracy.

6.2. Object Detection

The robustness of the object detection algorithm versus localization errors is evaluated, in order to check whether the achieved positioning accuracy is adequate to correctly associate objects detected by the on-board surveillance system. Specifically, one of the biggest problems to be taken into consideration during surveillance is that an object, which has been previously mapped and classified as “not dangerous”, can be used by a potential intruder to hide himself: a thief standing against a wall is a well-known example. Even if this latter case, in our system, is handled by the network of fixed sensors, the task assigned to robots is nevertheless critical: in spite of localization errors which can severely affect object matching (as described in Equation 1), the on-board surveillance system must be able to find the correct correspondences between objects with different shapes and dimensions. Figure 8 shows the a posteriori probability that a detected object (whose diameters varies from 0.5 m to 1 m in different experiments) is correctly matched against the corresponding object in the map, by imposing an increasing localization error. We can observe that: (i) the localization accuracy observed in experiments (≤ 2 m) is adequate to guarantee correct data association in most cases; (ii) correct data association decreases with localization error; (iii) correct data association increase with object diameter. These results are confirmed by experiments described in Figure 9: objects of different diameters (from 0.5 m to 1 m) are detected and matched against objects in the map when the robot is at different distances (from 10 m to 30 m). The experiments clearly show that the improvement in self-localization due to bias estimation in B-tests leads to improved correct data association rate.

| disp./diam. | 0,5m | 0,6m | 0,7m | 0,8m | 0,9m | 1m |
|-------------|------|------|------|------|------|------|
| 1m | 0,96 | 0,96 | 0,98 | 0,98 | 0,99 | 0,99 |
| 1,3m | 0,94 | 0,94 | 0,95 | 0,96 | 0,97 | 0,98 |
| 1,6m | 0,91 | 0,91 | 0,93 | 0,94 | 0,95 | 0,98 |
| 1,9m | 0,86 | 0,87 | 0,89 | 0,91 | 0,93 | 0,95 |
| 2,2m | 0,6 | 0,65 | 0,68 | 0,71 | 0,74 | 0,76 |
| 2,5m | 0,46 | 0,49 | 0,52 | 0,56 | 0,58 | 0,62 |

Figure 8. Object matching vs. localization accuracy.

| dist./diam. | | 0,5m | 0,6m | 0,7m | 0,8m | 0,9m | 1m |
|-------------|---------|------|------|------|------|------|-----|
| 10m | A-tests | 0,84 | 0,87 | 0,9 | 0,92 | 0,96 | 1 |
| | B-tests | 0,91 | 0,93 | 0,94 | 0,96 | 0,97 | 1 |
| 15m | A-tests | 0,76 | 0,79 | 0,83 | 0,86 | 0,9 | 0,9 |
| | B-tests | 0,9 | 0,91 | 0,93 | 0,95 | 0,96 | 1 |
| 20m | A-tests | 0,66 | 0,68 | 0,72 | 0,77 | 0,8 | 0,8 |
| | B-tests | 0,86 | 0,88 | 0,89 | 0,91 | 0,94 | 1 |
| 25m | A-tests | 0,46 | 0,49 | 0,52 | 0,56 | 0,59 | 0,6 |
| | B-tests | 0,79 | 0,81 | 0,83 | 0,86 | 0,9 | 0,9 |
| 30m | A-tests | 0,2 | 0,25 | 0,27 | 0,29 | 0,31 | 0,3 |
| | B-tests | 0,65 | 0,71 | 0,77 | 0,79 | 0,83 | 0,9 |

Figure 9. Object matching vs. localization accuracy.

7. Conclusions

The paper describes the capabilities of the mobile robot ANSER in terms of autonomous surveillance, localization and navigation.

In ANSER, great attention has been paid to the mutual role played by system specifications and system autonomy. Usually, complete autonomy is not desirable. On the opposite, a carefully designed trade-off must be set to balance surveillance policies and autonomous decision making. Specifically, autonomous surveillance requires to detect differences between perceived and expected environmental conditions, on the basis of a simple laser rangefinder based algorithm. To guarantee the necessary accuracy for navigation and surveillance, the localization subsystem plays a fundamental role. Instead of equipping the robot with a huge amount of expensive sensors, an augmented state vector approach is chosen that relies exclusively on a non-differential GPS unit and a laser rangefinder, and allows to estimate both the robot pose and the low frequency components of the GPS measurements. The experiments confirm the expectations, showing that the approach reasonably improves the overall system capabilities. Finally, a navigation algorithm is introduced (and its properties formally demonstrated) which proves to be very suited to the considered scenario, allowing smooth and stable trajectories even when moving at high speed.

References

- [1] T. HEATH-PASTORE, H.R. EVERETT, AND K. BONNER. Mobile Robots for Outdoor Security Applications. In *American Nuclear Society - 8th Int. Topical Meeting on Robotics and Remote Systems*, Pittsburgh, PA, 1999.
- [2] M. SAPTHARISHI, C.S. OLIVER, C.P. DIEHL, K.S. BHAT, J.M. DOLAN, A. TREBI-OLLENNU, P.K. KHOSLA. Distributed Surveillance and Reconnaissance Using Multiple Autonomous ATVs: Cyber-Scout. In *IEEE Trans. on Rob. and Autom.*, vol. 18, no. 5, 2002.
- [3] R. VIDAL, O. SHAKERNIA, H.J. KIM, D.H. SHIM, S. SASTRY. Probabilistic Pursuit-Evasion Games: Theory, Implementation, and Experimental Evaluation. In *IEEE Trans. on Rob. and Autom.*, vol. 18, no. 5, 2002.
- [4] I. VOLKAN, K. SAMPATH, K. SANJEEV. Randomized Pursuit-Evasion in a Polygonal Environment. In *IEEE Trans. on Robotics*, vol. 21, no. 5, 2005.
- [5] P.E. RYBSKI, S.A. STOETER, M. GINI, D.F. HOUGEN, N.P. PAPANIKOLOPOULOS. Performance of a Distributed Robotic System Using Shared Communications Channels. In *IEEE Trans. on Rob. and Autom.*, vol. 18, no. 5, 2002.
- [6] S. PANZIERI, F. PASCUCCI, G. ULIVI. An Outdoor Navigation System Using GPS and Inertial Platform. In *IEEE Trans. on Mechatronics*, vol. 7, no. 2, 2002.
- [7] T. SCHNBERG, M. OJALA, J. SUOMELA, A. TORPO, A. HALME. Positioning an Autonomous Off-Road Vehicle by Using Fused DGPS and Inertial Navigation. In *Proc. of the 2nd IFAC Conf. on Intelligent Autonomous Vehicles (IAV)*, Espoo, Finland, June 12–14, 1995.
- [8] G. DISSANAYAKE, S. SUKKARIEH, E. NEBOT, H. DURRANT-WHYTE. The Aiding of a low-cost Strap-down Inertial Measurement Unit Using Vehicle Model Constraints for Land Vehicle Applications. In *IEEE Trans. on Rob. and Autom.*, vol. 17, no. 5, pp. 731–747, 2001.
- [9] J.A. FARRELL, T. GIVARGIS, M. BARTH. Real-time Differential Carrier Phase GPS-aided INS. In *IEEE Trans. on Control and System Technology*, vol. 8, pp. 709–721, 2000.
- [10] J.Z. SASIADEK, Q. WANG. Low Cost Automation Using INS/GPS Data Fusion for Accurate Positioning. In *Robotica*, vol. 21, pp. 255 – 260, 2003.
- [11] F. CAPEZIO, F. MASTROGIOVANNI, A. SGORBISSA, R. ZACCARIA. Fast Position Tracking of an Autonomous Vehicle in Cluttered and Dynamic Indoor Environments. In *Proc. of the 8th Int. IFAC Symp. on Robot Control (SYROCO-06)*, Bologna, Italy, September 2006.
- [12] F. CAPEZIO, A. SGORBISSA, R. ZACCARIA. GPS-based Localization for UGV Performing Surveillance Patrols in Wide Outdoor Areas. In *Proc. of the 2005 Int. Conf. on Field and Service Robotics (FSR-05)*, Australia, July 2005.
- [13] A. FOD, A. HOWARD, M. MATARIC. Laser-based People Tracking. In *Proc. of the 2002 IEEE Int. Conf. on Rob. and Autom. (ICRA-02)*, Washington DC, May 2002.
- [14] D. SCHULTZ, W. BURGARD, D. FOX, A.B. CREMERS. People Tracking with Mobile Robots Using Sample-based Joint Probabilistic Data Association Filters. In *Int. J. of Robotics Research*, vol. 22, no. 2, pp. 99 – 116, 2003.
- [15] K.O. ARRAS, O.M. MOZOS, W. BURGARD. Using Boosted Features for the Detection of People in 2D Range Data. In *Proc. of the 2007 IEEE Int. Conf. on Rob. and Autom. (ICRA-07)*, Rome, Italy, April 2007.
- [16] M. AICARDI, G. CASALINO, A. BICCHI, AND A. BALESTRINO. Closed Loop Steering of Unicycle-Like Vehicles via Lyapunov Techniques. In *IEEE Rob. and Autom. Mag.*, 1995.
- [17] M.K. BUGEJA AND S.G. FABRI. Dual Adaptive Control for Trajectory Tracking of Mobile Robots. In *Proc. of the 2007 IEEE Int. Conf. on Rob. and Autom. (ICRA'07)*, Rome, Italy, April 10-14, 2007.

Received: December, 2007

Revised: April, 2008

Accepted: May, 2008

Contact addresses:

Francesco Capezio

Fulvio Mastrogiovanni

Antonio Sgorbissa

Renato Zaccaria

DIST, Department of Communication

Computer and System Sciences

University of Genova

Via Opera Pia 13

16145 Genova, Italy

e-mail: {francesco, fulvio, sgorbiss,

renato}@dist.unige.it

FRANCESCO CAPEZIO received a 5-year Engineering degree in Computer Science and the Ph.D. in Robotics from University of Genova, Italy. He is currently a Research Assistant at Department of Communication, Computer and System Sciences (DIST), University of Genova, Italy. His research addresses the field of mobile robot control, navigation and localization with a special interest on multi-robot coordination. He also works on sensor networks suitable to Ambient Intelligence applications.

FULVIO MASTROGIOVANNI received a 5-year Engineering degree in Computer Science and the Ph.D. in Robotics from University of Genova, Italy. He is currently Research Assistant at DIST, University of Genova, where he pursues research on the integration between Autonomous Robotics and Ambient Intelligence, with a special focus on sensing, information fusion and knowledge representation. Recently, his research focus is directed towards Humanoid Robotics and self-aware systems.

ANTONIO SGORBISSA received a 5-year degree in Electronic Engineering and the Ph.D. in Robotics from the University of Genova, Italy. Currently, he is Assistant Professor in Computer Science at the Faculties of Engineering and Humanities, University of Genova, and he leads the Mobile Robotics "Laboratorium" group at the Department of Communication, Computer, and System Sciences (DIST). His main research interests are intelligent autonomous systems, with a special focus on indoor and outdoor mobile robots, distributed multi-robot systems, planning, navigation and control.

RENATO ZACCARIA received a 5-year degree in Electrical Engineering from University of Genova, Italy. He is Full Professor in Computer Science at the Department of Communication, Computer and System Sciences (DIST), University of Genova, Italy, and the local Coordinator of EMARO, the European Master on Advanced Robotics. He started working on Robotics in the 70s in one of the earlier Italian research groups, characterised by a strong interdisciplinary approach. His present activity regards mainly Service Robotics. In 2000 he founded the spin-off company "Genova Robot", whose present R&D activities are strongly linked to academic research. He has been awarded the title "Commendatore della Repubblica" because of his activities in technology transfer in Robotics.
